

[13–15]. The minimum stratigraphic thickness of the Chelmsford Formation is 600 m, so that the depositional time required is >1 m.y. The fastest deposition rate of hemipelagic deposits is 300 m/m.y., so that 600-m thickness of the Onwatin Formation corresponds to >2 m.y. [15], and possibly as much as 6 m.y. (D. G. F. Long, personal communication, 1992). This amounts to a time interval of at least 3 m.y. between the Sudbury event and the tectonic deformation of the Whitewater Group and the SIC.

If the SIC was formed as an impact melt, the sequence of events proposed herein requires the SIC deform in the unconsolidated state, 3–10 m.y. after its intrusion. Plutons emplaced at mid to upper crustal levels are thought to take 1–10 m.y. to cool to the ambient wall-rock temperatures; however, consolidation of a pluton takes a fraction of that time [7]. Impact melt sheets of the size of the Igneous Complex would crystallize well within 1 m.y. of their formation [3]. This duration is shorter than the time interval required for the deposition of the Onwatin and Chelmsford Formations. Together with the evidence for magmatic folding of the SIC, this time constraint renders the impact melt hypothesis of the SIC untenable.

**References:** [1] Peredery W. V. and Morrison G. G. (1984) *Ont. Geol. Surv. Spec. Publ. 1*, 491–512. [2] Faggart B. E. et al. (1985) *Nature*, 230, 436–439. [3] Grieve R. A. F. et al. (1991) *JGR*, 96, 22753–22764. [4] Stauffer M. R. (1988) *Tectonophysics*, 149, 339–343. [5] Lisle R. J. et al. (1990) *Tectonophysics*, 172, 197–200. [6] Paterson S. R. et al. (1989) *J. Struct. Geol.*, 11, 349–363. [7] Paterson S. R. et al. (1991) *Min. Soc. Am. Rev. Min.*, 26, 673–722. [8] Schwerdtner W. M. et al. (1983) *J. Struct. Geol.*, 5, 419–430. [9] Cantin R. and Walker R. G. (1972) *Geol. Ass. Can. Spec. Pap. 10*, 93–101. [10] Rousell D. H. (1984) *Ont. Geol. Surv. Spec. Pub. 1*, 211–218. [11] Long D. G. F., this volume. [12] Shanks W. S. and Schwerdtner W. M. (1991) *Can. J. Earth Sci.*, 28, 411–430. [13] Ricci Lucci F. and Valmori E. (1980) *Sedimentology*, 27, 241–270. [14] Hiscott R. N. et al. (1986) *Int. Assoc. Sediment. Geol. Spec. Publ. 8*, 309–325. [15] Pickering K. T. et al. (1989) *Deep Marine Environments*, Unwin Hyman, 416 pp.

475163  
517-46  
N93581 0129  
B 1720314

**ENHANCED MAGNETIC FIELD PRODUCTION DURING OBLIQUE HYPERVELOCITY IMPACTS.** D. A. Crawford and P. H. Schultz, Department of Geological Sciences, Brown University, Providence RI 02912, USA.

The natural remanent magnetization of the lunar surface as displayed in returned lunar samples and the data returned by the Apollo subsatellite magnetometer has an unexpectedly high magnitude and exhibits spatial variation at all scales. The origin of the lunar remanent fields may be due to crustal remanence of a core dynamo field occurring early in lunar history prior to extensive modification by impact [1] or remanence of transient fields, particularly associated with impacts, occurring on a local scale throughout lunar history [2–5]. The presence of an early core dynamo field would have strong consequences for the formation and early evolution of the Moon, yet to deconvolve the role that an internally generated core dynamo field may have had, it is necessary to understand how the magnetic state of the lunar surface has developed through time. Impact-induced magnetism may be an important component of the present magnetic state of the lunar surface.

New theoretical considerations suggest that transient magnetic fields within plasma produced by hypervelocity meteorite impacts may have greater significance at larger scales than previously thought [6]. Self-similar, one-dimensional solutions for the evolu-

tion of the magnetic field and electron energy within impact-generated plasma demonstrate that the peak magnetic field strength may only weakly depend on projectile size. Because the ratio of projectile size to crater size increases at larger scales for gravity-limited growth, the peak strength of transient impact-generated magnetic fields probably increases with increasing crater size at the same diameter-scaled distance. A conservative estimate (from extrapolated experimental data) for 10–100-km craters formed by vertically incident meteorite impacts at 25 km/s predicts magnetic field strengths of at least 0.03–0.1 G for several minutes or more [6]. This is within the range of paleointensity values determined for certain relatively young (3 Ma to 1.5 Ga) lunar samples [7–9] and more generally may help account for the lunar magnetic record during the last ~3.5 b.y. Recently acquired experimental evidence suggests that impact at oblique incidence may further enhance magnetic field production by as much as an order of magnitude.

Experimental investigations of magnetic field generation and evolution during hypervelocity impacts have been conducted at the NASA Ames Vertical Gun Range, Moffett Field, California [10–12]. The vertical gun is a two-stage hydrogen light gas gun capable of launching macroscopic projectiles at up to 7 km/s with the angle of impact varying from nearly horizontal to vertical in increments of 15°. The large impact chamber, which can be evacuated to less than ~1 Torr, is large enough to accommodate, surrounding the impact point, a mu-metal shield that reduces the 35- $\mu$ T terrestrial magnetic field to  $450 \pm 80$  nT—comparable to lunar surface field strength.

Impacts of aluminum projectiles into powdered dolomite ( $Mg_0.5Ca_0.5CO_3$ ) targets readily produce a self-luminescent, slightly ionized vapor cloud that we infer to be the source of impact-generated magnetic fields [3,6]. Oblique impacts demonstrate enhanced vapor yield producing a vapor cloud that retains a portion of the impactor momentum with a leading edge that travels downrange at a significant fraction of the impact velocity [13].

The configuration and duration of impact-generated magnetic fields observed during laboratory hypervelocity impacts are strongly dependent on impact angle (Figs. 1–3). Magnetic search coil data from many experiments under identical impact conditions were combined to produce the plots shown. The observed magnetic fields exhibit a regular transition from a cylindrically symmetric field configuration at vertical incidence to a strong bilaterally antisymmetric field configuration at high obliquity (Figs. 1 and 2). The stronger magnetic fields observed during oblique impacts (see Fig. 3) could result simply from the close proximity of impact-generated plasma to the target surface, from a fundamental change in the field production mechanism within the plasma or from increased vaporization [13] yielding a greater volume of magnetized plasma; however, this could not be resolved with the data obtained. In addition to impact angle, experiments demonstrate that the configuration and duration of impact-generated magnetic fields are dependent on impact velocity and projectile/target composition [11].

A remnant of the impact-generated magnetic field could be induced within the target material during passage of the impact-induced shock wave [14,15] or by cooling through the Curie point of small portions of impact melt or hot target material. During oblique impacts, spalled fragments of the projectile may impact further downrange at hypervelocities [16], thereby inducing a shock and/or thermal remanence significantly offset from the crater rim. Because of these dependencies, remnant impact-generated magnetic fields could be a useful geophysical tool for the study of impact craters on the Earth and planetary surfaces by helping to determine the impact angle, direction, and composition of impactors. The

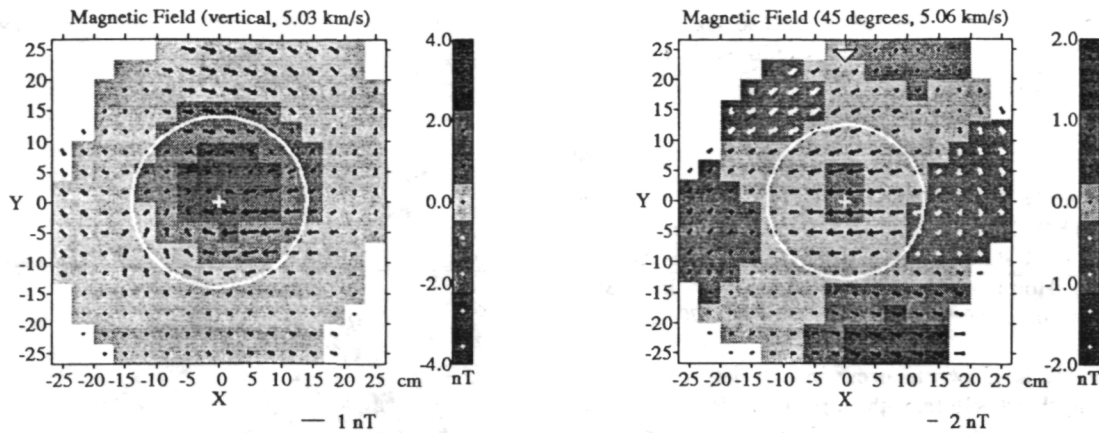


**Fig. 1.** Average magnetic field observed during the time interval 0.3–0.5 ms after hypervelocity ( $\sim 5$  km/s) impacts of 0.64-cm aluminum projectiles into powdered dolomite targets. Each plot represents the magnetic field as seen in a horizontal plane 9 cm below a vertical impact (left) and an oblique impact,  $45^\circ$  from horizontal (right). Shading represents the vertical component of the field whereas vectors represent the horizontal component with white vectors appearing where the field is directed into the page (down). The crater (shown as a white circle) defines the origin (shown as a white cross) of the coordinate system. A white triangle indicates the projectile trajectory prior to impact.

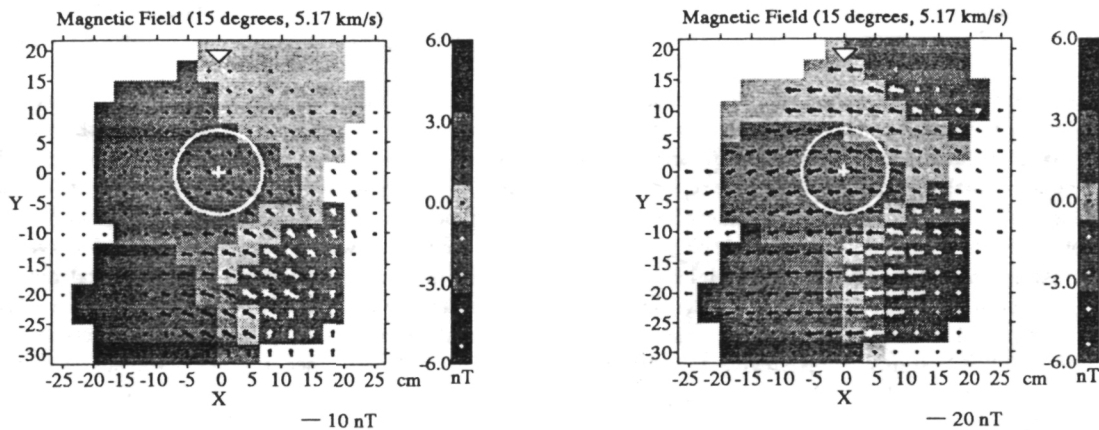


**Fig. 2.** Magnetic field during an oblique  $15^\circ$  impact at the same time as in Fig. 1 (left) and 0.4 ms later (right).

many possible time-dependent impact-related magnetic field patterns and the various possible remanence acquisition mechanisms (some or all of which may come into play during a given impact event) yield a broad spectrum of possible crater-related remnant field patterns. An understanding of this complex contribution of impact-induced magnetism to the magnetic state of solid body surfaces, in general, and the lunar surface, in particular, is necessary to assess the role of internally derived fields such as from a core dynamo and may help to define future magnetic survey missions to solid surface planets, satellites, and asteroids.

**References:** [1] Runcorn S. K. (1983) *Nature*, 304, 589–596. [2] Gold T. and Soter S. (1976) *Planet. Space Sci.*, 24, 45–54. [3] Srnka L. J. (1977) *Proc. LSC 8th*, 893–895. [4] Schultz P. H. and Srnka L. J. (1980) *Nature*, 284, 22–26. [5] Hood L. L. and Huang Z. (1991) *JGR*, 96, 9837–9846. [6] Crawford D. A. (1992) *JGR*, submitted. [7] Sugiura N. et al. (1979) *Proc. LPSC 10th*, 2189–2197. [8] Cisowski S. M. et al. (1983) *Proc. LPSC 13th*, in *JGR*, 88, A691–A704. [9] Collinson D. W. (1984) *PEPI*, 34, 102–116. [10] Crawford D. A. and Schultz P. H. (1988) *Nature*, 336, 5052. [11] Crawford D. A. and Schultz P. H. (1991) *JGR*, 96, 18807–18817. [12] Crawford D. A. and Schultz P. H. (1992) *LPSC XXIII*, 259–260. [13] Schultz P. H. (1988) *LPSC IX*, 1039–1040. [14] Cisowski S. M.

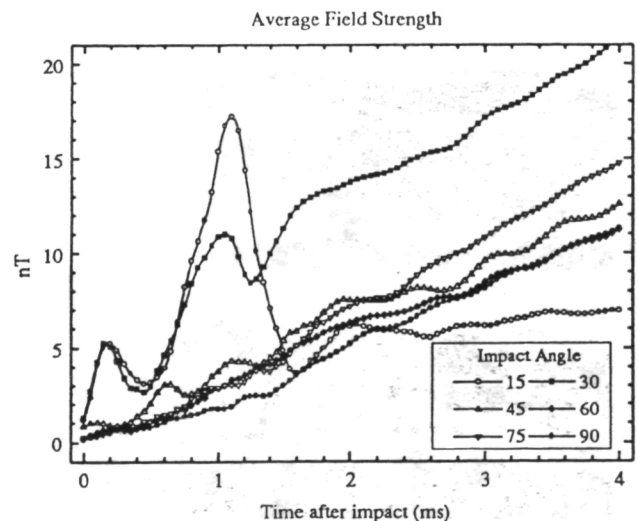


**Fig. 3.** Spatially averaged magnetic field strength as a function of time after impact. Results from six impact angles are shown. Enhanced field production during the first millisecond after impact is apparent for oblique impacts at  $15^\circ$  and  $30^\circ$  from horizontal.

et al. (1975) *Proc. LSC 6th*, 3123–3141. [15] Cisowski S. M. et al. (1976) *Proc. LSC 7th*, 3299–3320. [16] Schultz P. H. and Gault D. E. (1990) *GSA Spec. Pap.* 247.

518-46 116 3093 #10130 475164  
**IMPACTITE AND PSEUDOTACHYLITE FROM ROTER KAMM CRATER, NAMIBIA.** J. J. Degenhardt Jr.<sup>1,2</sup>, P. C. Buchanan<sup>1</sup>, and A. M. Reid<sup>1</sup>, <sup>1</sup>Department of Geosciences, University of Houston, Houston TX 77204, USA, <sup>2</sup>Texaco Inc., E&P Technology Division, 3901 Briarpark, Houston TX 77042, USA.

Pseudotachylite is known to occur in a variety of geologic settings including thrust belts (e.g., the Alps and the Himalayas) and impact craters such as Roter Kamm, Namibia. Controversy exists, however, as to whether pseudotachylite can be produced by shock brecciation [1] as well as by tectonic frictional melting. Also open to debate is the question of whether pseudotachylites form by frictional fusion or by cataclasis [2]. It has been speculated that the pseudotachylite at Roter Kamm was formed by extensional settling and adjustment of basement blocks during "late modification stage" of impact [3]. The occurrence of pseudotachylite in association with rocks resembling quenched glass bombs and melt breccias in a relatively young crater of known impact origin offers a rare opportunity to compare features of these materials. Petrographic, X-ray diffraction, and electron microprobe analyses of the impactites and pseudotachylite are being employed to determine the modes of deformation and to assess the role of frictional melting and comminution of adjacent target rocks. The first findings are reported here.

The Roter Kamm Crater is located in the southern part of the Namib Desert about 80 km north of Oranjemund, Namibia. The crater rim has a crest diameter of ca. 2.5 km with the highest exposed point reaching 158 m above the lowest point of the crater floor. The impact, which excavated Precambrian granitic-granodioritic orthogneisses of the 1200–900-m.y.-old Namaqualand Metamorphic Complex, has been dated at 3.5–4.0 Ma by Hartung et al. [4]. No volcanic rocks have been discovered in the area [5]. This has been substantiated by others [3]. A detailed account of the crater geology was published by Reimold and Miller [6].

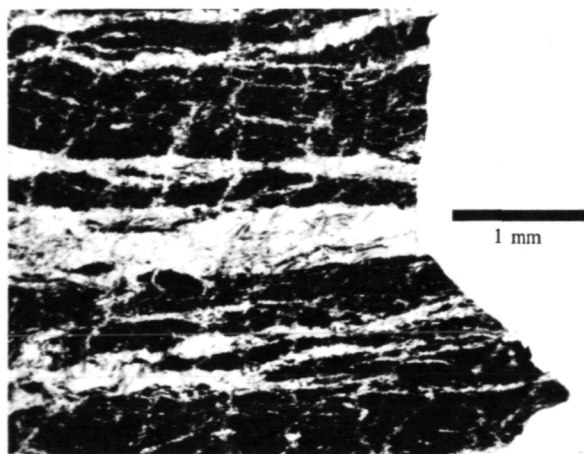


**Fig. 1.** Photomicrograph of flädle in transmitted light illustrating veinlets of subhedral mica and quartz set in opaque matrix. Veinlets terminate abruptly at edge of sample.

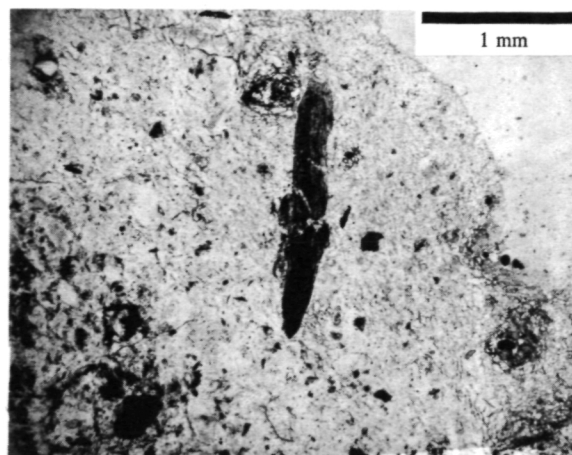


**Fig. 2.** Plane light photomicrograph of opaque clasts entrained in quartz breccia matrix. Large clast (center) is 1.6 mm in length.

A variety of impactites was collected from the crater rim. These have been described in the literature as "impact-melt breccias," "melt bombs," and "ejecta melts." In this study, three main rock types have been examined:

1. Meltlike rocks (also called flädle), common only along the northwest crater rim, are dark gray to black in color and exhibit apparent flow patterns characteristic of quenched glass "bombs." Because of their smooth, fluidlike shapes, the flädle have been interpreted as impact melt. In spite of their meltlike appearance, the specimens that were examined exhibited pervasive subparallel millimeter-wide veinlets containing subhedral mica and quartz. The fact that these veins are sharply (visibly) truncated by the surfaces of the flädle brings into question the interpretation that these rocks were melt-derived (see Fig. 1). XRD and electron microprobe analyses of the veins confirmed the mica-quartz composition and showed the mica to be a K, Mg-bearing variety. The finer-grained, optically opaque matrix is composed of mica and quartz similar to that of the veins. A Ti-rich mineral was also found to be present in the matrix, mainly in the form of clustered grains scattered throughout. Further analysis is being carried out to determine the cause of the opacity.

2. Quartz breccias containing large irregular shocked quartz fragments were also collected along the north crater rim. The fragments are cemented by an aphanitic matrix that resembles pseudotachylite in hand specimen. In contrast to the flädle, this matrix is not opaque in thin section, but appears finely crystalline. Of significance is the presence of opaque clasts (some containing micaceous veins) located throughout the matrix, which upon preliminary examination appear to be composed of the same material as the flädle (Fig. 2). Work is currently being done to determine if the chemical compositions of these entrained clasts match that of the flädle, and thus whether the flädle material predates the quartz breccia.

3. Pseudotachylite samples in the form of allochthonous fragments were collected at the south rim. Petrographic examination reveals the presence of angular entrained clasts that have not undergone recrystallization. However, finely crystalline quartz resembling the quartz breccia matrix appears in (plastically?) deformed grains and intermediate zones that often separate the pseudotachylite from its host rock. The composition of the vein material, including nonrecrystallized entrained clasts, was found to